Available online at www.sciencedirect.com
ScienceDirect
Journal of Organometallic Chemistry 691 (2006) 4411–4418
Journal of Organometallic Chemistry
www.elsevier.com/locate/jorganchem

(*P*-Bis(pentafluorophenyl) substituted) PCP-pincer Ru(II) complexes: A theoretical study of the molecular structure and electronic properties

Marcella Gagliardo [a], Remco W.A. Havenith [b,1], Gerard van Klink [a], Gerard van Koten [a,*]

[a] *Debye Institute, Organic Chemistry and Catalysis, Utrecht University, Padualaan 8, 3584 CH Utrecht, The Netherlands*
[b] *Debye Institute, Theoretical Chemistry Group,[2] Utrecht University, Padualaan 8, 3584 CH Utrecht, The Netherlands*

Received 20 October 2005; received in revised form 16 December 2005; accepted 3 January 2006
Available online 9 March 2006

Abstract

The differences between the molecular structures of the PCP-pincer complex $[RuCl\{C_6H_3(CH_2P(C_6H_5)_2)_2\text{-}2,6\}(PPh_3)]$ ($[RuCl(PCP^H)(PPh_3)]$, **1**) and its tetrakis-pentafluorophenyl substituted analogue $[RuCl\{C_6H_3(CH_2P(C_6F_5)_2)_2\text{-}2,6\}(PPh_3)]$ ($[RuCl(PCP^{F20})(PPh_3)]$, **2**) have been rationalised by performing calculations on the cations $[Ru(PCP^H)(PPh_3)]^+$ (**1cat**) and $[Ru(PCP^{F20})(PPh_3)]^+$ (**2cat**). The molecular interactions between the chloride ligand and the axial rings, as found in **1** and **2**, respectively, have been studied computationally in the model systems $[(C_6X_5PH_2)_2Cl^-]$ (X = H, F). The calculations on **2cat** show that in **2** it is most likely the attractive electrostatic interaction between the chloride ligand and the fluorinated phenyl rings that forces the C_{ipso} atom to occupy an axial position rather than an equatorial one in the observed (X-ray of **2**) square pyramidal arrangement. In **1**, however, repulsive steric hindrance forces the PPh_3 ligand to take the apical position. The applicability of the TD-DFT method for the calculation of the electronic spectra of the PCP-pincer compounds **1** and **2** has been tested. The results indicate that the excitation energies calculated for both complexes are in a reasonable agreement with the experimental absorption maxima. However, for **1**, all the calculated transition energies are underestimated.

Keywords: DFT and ab initio calculations; Electrostatic interactions; PCP pincer ligands; Ruthenium(II)

1. Introduction

Late transition metal complexes containing monoanionic, terdentate coordinating PCP-pincer ligands ($[C_6H_3(CH_2PR_2)_2\text{-}2,6]^-$) are increasingly applied as catalysts in various organic transformations [1]. Among them, square-pyramidal PCP–Ru(II) complexes, incorporating electron-donating alkyl and aryl substituents on the phosphorus donor atoms, have attracted considerable attention due to their versatile catalytic activity [2]. In particular, the complexes $[RuCl\{C_6H_3(CH_2PPh_2)_2\text{-}2,6\}(PPh_3)]$ ($[RuCl(PCP^H)(PPh_3)]$, **1**, Fig. 1) [3] and $[RuCl\{C_6H_3(CH_2PCy_2)_2\text{-}2,6\}(PPh_3)]$ [4] were found to be very active in the reduction of ketones to the corresponding alcohols.

Fine tuning of the electronic and steric properties of PCP-pincer compounds is a topic of current interest. Recently, it was shown that the introduction of strong π-accepting substituents to the ruthenium centre has a profound impact on the molecular structure and reactivity of corresponding PCP-pincer complexes [5,6].

We reported the synthesis of a novel, monoanionic strongly π-accepting ligand $[C_6H_3(CH_2P(C_6F_5)_2)_2\text{-}2,6]^-$ (PCP^{F20}) [7] and some aspects of its chemistry with palladium [7] and ruthenium [6]. It was pointed out that the fluorinated complex $[RuCl(PCP^{F20})(PPh_3)]$ (**2**, Fig. 1) is remarkably air and moisture stable. The redox and electronic properties, as well as the structural features of **2** differ significantly from those of its protio analogue **1** [8]

* Corresponding author. Tel.: +31 30 253 3120; fax: +31 30 252 3615.
E-mail addresses: r.w.a.havenith@chem.uu.nl (R.W.A. Havenith), g.vankoten@chem.uu.nl (G. van Koten).
[1] Author to whom theoretical calculations inquiries may be directed.
[2] Affiliated to Organic Chemistry and Catalysis.

0022-328X/$ - see front matter © 2006 Elsevier B.V. All rights reserved.
doi:10.1016/j.jorganchem.2006.01.035

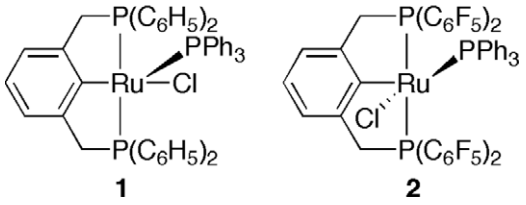

Fig. 1. Monoanionic, terdentate coordinating PCP-pincer ruthenium complexes [RuCl{$C_6H_3(CH_2PPh_2)_2$-2,6}(PPh_3)] (**1**) and [RuCl{C_6H_3-$(CH_2P(C_6F_5)_2)_2$-2,6}(PPh_3)] (**2**).

(Fig. 1) and other PCP-pincer Ru(II) complexes [4,9]. In the distorted square-pyramidal molecular geometry of **1** (Fig. 2, left), the PPh_3 ligand occupies the apical position, while the other two phosphorus centres, together with the chloride and the C_{ipso} atom form the base of the square pyramidal configuration. The complex has a mirror type arrangement of the two fused five member chelate rings. The phosphorus centre in each of the puckered chelate rings has one phenyl ring equatorially and one axially (opposite to the apical PPh_3 ligand) oriented [8]. Jia and co-workers postulated that the geometry of **1** is strongly influenced by steric factors and that the crowding between the PCP ligand and PPh_3 is minimised in the resulting structure, in which the PPh_3 takes the apical position [8a].

Contrary to this assumption, substitution of the PCP^H ligand by PCP^{F20} does not change the metal coordination environment in the molecular structure of **2** (Fig. 2, right) [6]. Similarly to what was found for **1**, also in complex **2** the C_6F_5-rings have an axial/equatorial positioning. The crystal structure of **2** shows the ruthenium centre to be in a distorted square-pyramidal geometry. However, it now appears that the PCP^{F20} ligand adjusted its effective bulkiness by promoting the migration of the chloride in a position *trans* to the PPh_3. This results in the apical position being occupied by C_{ipso} while the basal plane is formed by the three phosphine groups and the chloride [6]. Hindered rotation between the phenyl rings of the PPh_3 and the C_6F_5 axial rings observed in solution for **2** by temperature dependent ^{19}F NMR, is in line with the larger overall steric bulk of C_6F_5 versus C_6H_5 [6]. Yet, in the molecular structure of **2**, C_{ipso} of the cyclometalated PCP^{F20}-pincer ligand rather than the PPh_3 takes the apical position.

The motivation of the work presented in this paper was to investigate the observed structural changes in complex **2** compared to **1** and to rationalise why the replacement of C_6H_5- by C_6F_5-groups determines the preference of the σ-donating aryl ligand to occupy an axial, rather than an equatorial position.

Theoretical calculations showed that attractive electrostatic interactions exist between perfluoro aromatic compounds, such as hexafluorobenzene, and several anions [10]. These results prompted us to investigate whether this type of interaction is present in **1** and **2** and to which extent this can influence the geometry of PCP-pincer Ru(II) complexes.

Here, we report a theoretical study carried out on model systems for **1** and **2**, demonstrating how the structural features of **1** and **2** are governed by Coulomb interactions between the chloride ligand and the phenyl rings of the phosphorus atoms of the PCP-pincer ligand. The TD-DFT is a very popular approach for calculating electronic excitation spectra and has been applied to various molecular systems [11]. However, it has been proven that the applicability of this method to medium-sized and large metal-containing molecules is still limited [11]. The applicability of the TD-DFT method in the interpretation of the UV–Vis spectra of **1** and **2** is evaluated. Thus, these fundamental knowledges may allow for a better understanding of the photophysical properties of novel energy transfer systems incorporating photo- and redox active organometallic PCP-pincer Ru(II) building blocks [12].

2. Computational details

Geometries of **1** and **2** were optimised with GAMESS-UK [13] at the B3LYP level of theory. The LANL2-DZ basis set was selected for ruthenium, and for the other atoms the SV Dunning basis set was used [14]. Natural

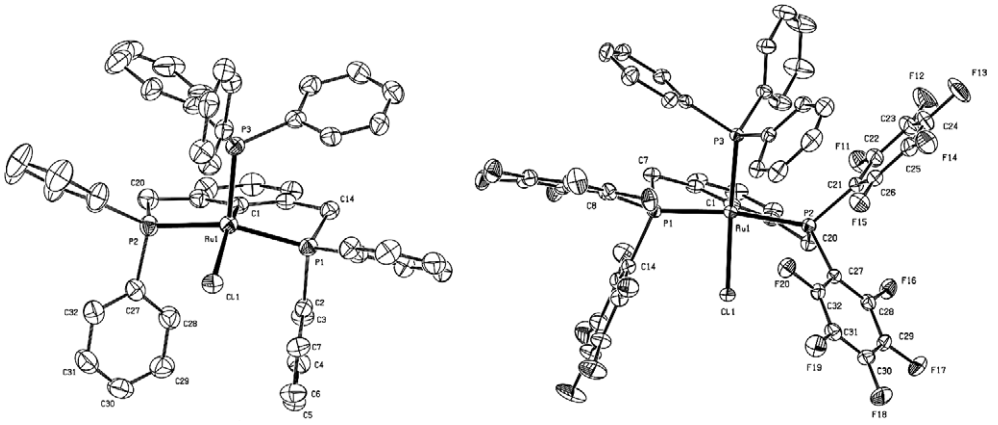

Fig. 2. ORTEP drawings (30% probability atomic displacement ellipsoid) of **1** (left) and **2** (right) [6]. Hydrogen atoms have been omitted for clarity.

population analysis (NPA) [15] was performed with the NBO-3.0 program [16] as implemented in GAMESS-UK.

To clarify which factors force the ligands in **2** to adopt the observed coordination geometry, four models have been constructed. All models ($[(C_6X_5PH_2)_2Cl]^-$, X = H, F; vide infra, Fig. 5) are composed of two phosphorus atoms each with its axial phenyl ring and the chloride anion positioned according to their orientation in **1** or **2**. In all models the P–H bond lengths were chosen to be 1.42 Å. The two model compounds **m1** have been constructed in such a manner that the two rings are, with respect to each other, in the same position that they have in **1** and with the chloride anion *trans* to C_{ipso}. While **m1-H** contains two C_6H_5-rings ($[(C_6H_5PH_2)_2Cl]^-$), **m1-F** has two C_6F_5-rings ($[(C_6F_5PH_2)_2Cl]^-$; C–F length fixed at 1.38 Å). Analogously, also in the two model compounds **m2**, the phenyl rings are positioned with the respect to each other as they are in **2**, having the chloride anion positioned in between. Again, **m2-H** contains two C_6H_5-rings ($[(C_6H_5PH_2)_2Cl]^-$; C–H bond length fixed at 1.08 Å), **m2-F** has two C_6F_5-rings ($[(C_6H_5PH_2)_2Cl]^-$).

The interaction energies between the chloride ion and the two aryl $C_6X_5PH_2$ (X = H, F) rings, were calculated at the MP2/cc-pVTZ levels of theory. The calculated interaction energies were corrected for the basis set superposition error (BSSE) [17] using the counterpoise procedure [18]. Polarisation dispersion energies were determined following the procedure outlined in Ref. [19], and the interaction energies between the fragments were further analysed in Coulomb and exchange energies using the Morokuma analysis of the RHF reference wave function [20].

The UV–Vis spectra were calculated using the TD-DFT approach and were performed with DALTON [21]. The LANL2-DZ basis set was used for the ruthenium atom, and the SV Dunning basis set on the other atoms [14]. The first 10 excited states were determined and only those with an oscillator strength larger than 0.002 are mentioned in the text.

3. Results and discussion

3.1. Molecular geometries and charge distribution

In Fig. 3, the optimised geometries for **1** and **2** are shown, together with NPA [15] charges on selected atoms. Comparison between the geometry optimization results with the available experimental X-ray [6] data show that the bond lengths and angles in **1** and **2** are reproduced quite well (Table 1). The general trends observed in the experimental geometries are well reproduced by the calculated ones (Table 1). Thus, a change in relative orientation of the chloride, a significant shortening of the Ru–Cl bond and a lengthening of the Ru–PPh_3 bond are observed in **2** compared to **1**. For both **1** and **2**, the NPA charges on the chloride are negative (Fig. 3). The charge inversion that occurs at the carbon atoms of the fluorinated aryl rings in **2** reflects the higher electronegativity of the fluorine atoms compared to the hydrogen atoms.

As a first attempt to explain why the chloride anion occupies a different position upon fluorination of the phenyl rings, we carried out calculations on the cations of **1** ($[Ru(PCP^H)(PPh_3)]^+$, **1cat**) and **2** ($[Ru(PCP^{F20})(PPh_3)]^+$, **2cat**). The geometries of **1cat** and **2cat** are very similar (a selection of calculated bond lengths and angles is reported in Table 2), as well as their frontier orbitals (Fig. 4).

The LUMO points to the position *trans* to the PPh_3 ligand in both cations, suggesting that the chloride anion would preferably bind in this position. Indeed, the chloride occupies this position in **2**. However, in **1**, the chloride occupies the position to which in **1cat** the LUMO + 1 points, i.e., *trans* to C_{ipso} (Fig. 4). In both cations the energy gap between the LUMO and the LUMO + 1 is

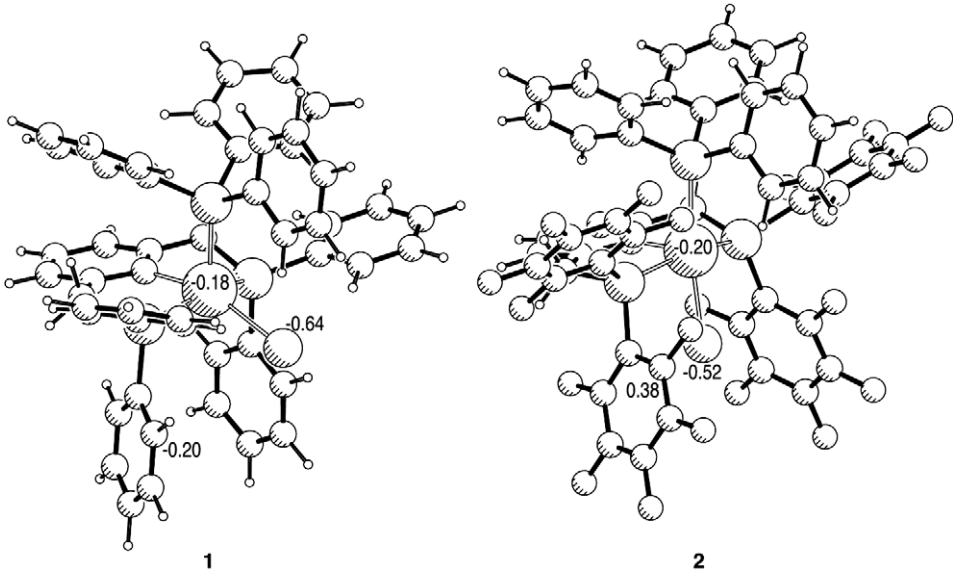

Fig. 3. B3LYP optimised geometries of **1** and **2**. Natural population charges on Ru, Cl, and Ph–C are indicated.

Table 1
Comparison of selected calculated bond lengths (Å) and angles (°) for **1** and **2** with corresponding experimental crystallographic data [6]

Bond length[a]	Calculated	Experimental	Angle[a]	Calculated	Experimental
*Compound **1***					
Ru(1)–C(1)	2.080	2.0730	P(1)–Ru(1)–P(2)	151.21	154.87
Ru(1)–P(1)	2.394	2.3039	Cl(1)–Ru(1)–P(3)	121.08	121.08
Ru(1)–P(2)	2.395	2.2937	Cl(1)–Ru(1)–C(1)	153.35	157.19
Ru(1)–P(3)	2.358	2.2174	Cl(1)–Ru(1)–P(1)–C(1)	−157.40	−154.03
Ru(1)–Cl(1)	2.590	2.4797	Cl(1)–Ru(1)–P(2)–C(1)	157.0	156.65
			P(1)–Ru(1)–C(1)–P(3)	−100.7	−103.06
			P(2)–Ru(1)–C(1)–P(3)	98.7	99.11
*Compound **2***					
Ru(1)–C(1)	2.058	2.0330	P(1)–Ru(1)–P(2)	159.0	155.42
Ru(1)–P(1)	2.394	2.2905	Cl(1)–Ru(1)–P(3)	166.9	166.93
Ru(1)–P(2)	2.395	2.3410	Cl(1)–Ru(1)–C(1)	96.46	95.24
Ru(1)–P(3)	2.358	2.3154	Cl(1)–Ru(1)–P(1)–C(1)	−96.2	−96.81
Ru(1)–Cl(1)	2.484	2.4121	Cl(1)–Ru(1)–P(2)–C(1)	96.1	97.50
			P(1)–Ru(1)–C(1)–P(3)	−96.6	−91.51
			P(2)–Ru(1)–C(1)–P(3)	98.5	95.13

[a] See Fig. 2.

Table 2
Selected calculated bond lengths (Å) and angles (°) for **1cat** and **2cat**

Bond length		Angle	
1cat			
Ru–C_{ipso}	2.040	PPh_2–Ru–PPh_2	155.54
Ru–PPh_2	2.410/2.416	PPh_3–Ru–C_{ipso}	92.44
Ru–PPh_3	2.366	PPh_2–Ru–C–PPh_3	−100.8/99.1
2cat			
Ru–C_{ipso}	2.043	$P(C_6F_5)_2$–Ru–$P(C_6F_5)_2$	158.41
Ru–$P(C_6F_5)_2$	2.431/2.435	PPh_3–Ru–C_{ipso}	97.55
Ru–PPh_3	2.394	PPh_2–Ru–C–PPh_3	−97.4/99.2

rather small, yet smaller in **1cat** ($\Delta E = 0.57$ eV) than in **2cat** ($\Delta E = 0.99$ eV). This suggests that **1cat** is more indifferent to the position of the incoming nucleophile than **2cat**.

The obtained results do not provide an answer to our question on the position of the chloride. Therefore, additional calculations on the interaction between the chloride and the two axial phenyl rings in its vicinity may explain the different bonding modes of the chloride. Four models have been constructed (Fig. 5). Models **m1-H** ($[(C_6H_5PH_2)_2Cl]^-$) and **m2-H** ($[(C_6H_5PH_2)_2Cl]^-$) have been made in order to match the orientation of the two axial C_6H_5-rings and the chloride in the geometries of **1** and **2**, respectively. Analogously, in the models **m1-F** ($[(C_6F_5PH_2)_2Cl]^-$) and **m2-F** ($[(C_6F_5PH_2)_2Cl]^-$) the orientation of the two axial C_6F_5-rings and the chloride correspond to what was found in the geometry of **1** and **2**, respectively.

The interactions between the chloride and the $C_6H_5PH_2$-moieties are small in both **m1-H** and **m2-H**. However, in the relative geometry of **1** it still attractive. Importantly, the interaction between the chloride and the $C_6F_5PH_2$-moieties is only repulsive in the geometry that matches that of **1**, and attractive in the orientation that matches that of **2**.

The MP2 interaction energy includes the polarization energy. For all the complexes a considerable dispersion energy is found (Table 3). The RHF interaction energies are naturally more repulsive than those evaluated at the MP2 level. The polarisation dispersion energies lowers the repulsion interaction energy significantly, and make the interaction in **m2-F** more favourable. The dispersion energy is largest for the **m2-H** and **m2-F** models, with the ion situated between the two phenyl-rings.

The attractive interaction found at the RHF level for **m2-F**, suggests an attractive electrostatic interaction between the chloride and the $C_6F_5PH_2$-moieties, whereas the interaction between the chloride and the $C_6H_5PH_2$-moieties is highly unfavourable. These findings are in accordance with the work reported by Alkorta et al. [10].

Further partitioning of the RHF interaction energies using the Morokuma scheme [20] is presented in Table 4. Note that the total RHF interaction energies shown in Table 4 are less repulsive than those in Table 3, due to the inclusion of BSSE correction [17] in the latter.

A survey of the energy contributions (Table 4) reveals that in both relative geometries, upon fluorination, the electrostatic contribution becomes attractive. Fluorination leads only to an increase in exchange repulsion in the relative geometry of **1**. The other contributions remain practically identical upon fluorination. Apparently, substitution of hydrogen for the electronegative fluorine atoms in the phenyl rings leads to a significant charge separation. The latter can favourably interact with the chloride when it is placed between the two rings, as is the case in **m2**. The exchange repulsion (steric hindrance) is not influenced by this substitution. Hence, **m2-F** is stabilised with respect to **m2-H** by Coulomb interactions. Although the electrostatic interaction is favourable for **m1-H**, the increase in exchange energy compensates for this attraction: the fluorine atoms are in too close contact with the chloride. Comparison of the contributions for **m1-H** and **m2-H** shows that, although a decrease in electrostatic energy is found, the exchange contribution increases dramatically, preventing this geometry to be energetically favourable. For **m2-F**,

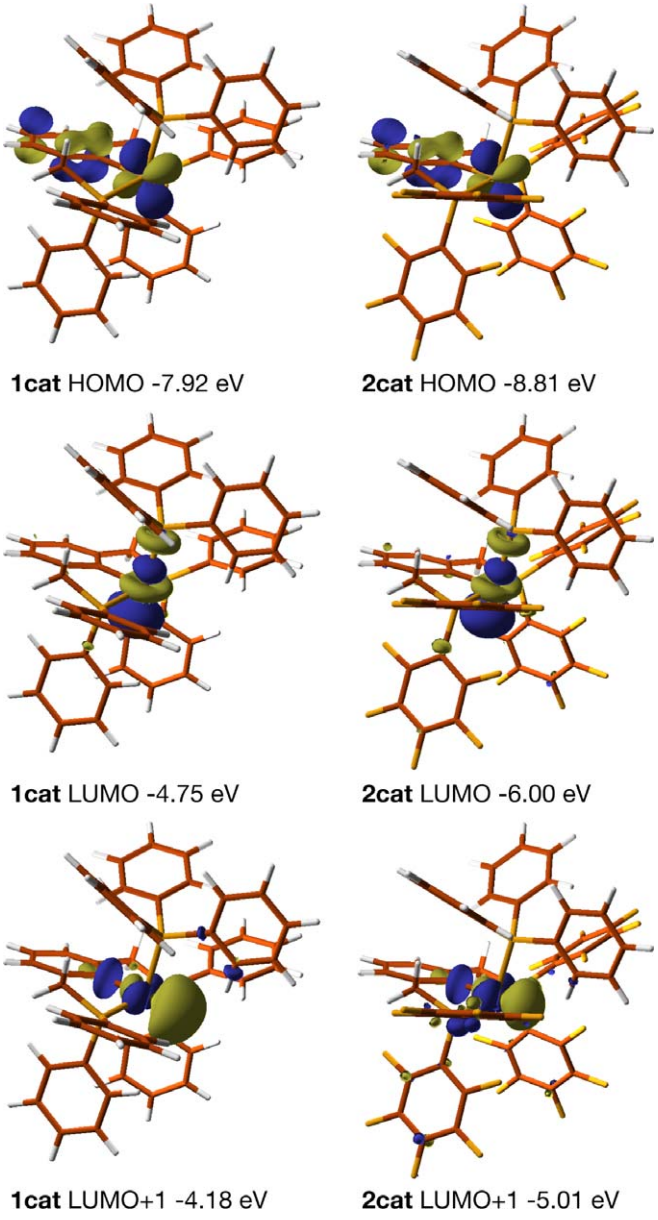

Fig. 4. Selected frontier orbitals of **1cat** ($[Ru(PCP^{H})(PPh_3)]^+$) and **2cat** ($[Ru(PCP^{F20})(PPh_3)]^+$).

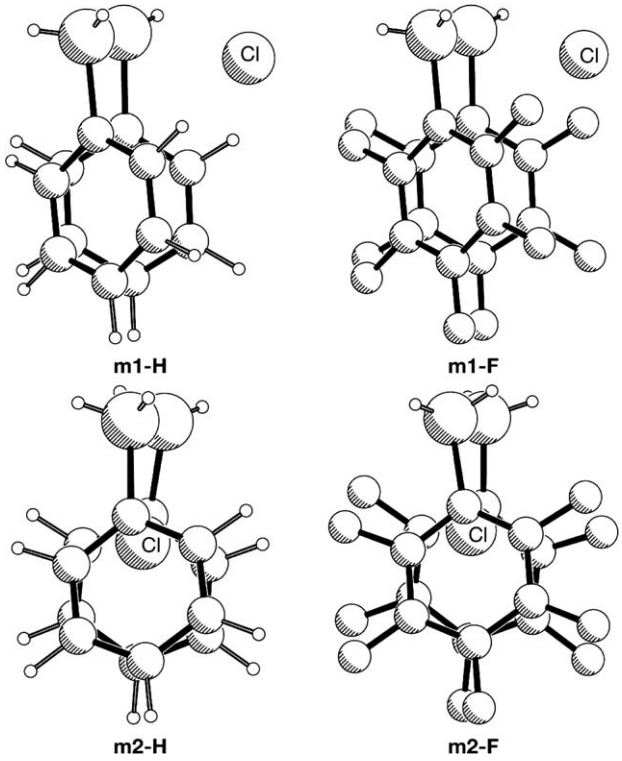

Fig. 5. Representation of the two **m1** models ($[(C_6X_5PH_2)_2Cl]^-$, X = H (**m1-H**), F (**m1-F**)) and the two **m2** models ($[(C_6X_5PH_2)_2Cl]^-$, X = H (**m2-H**), F (**m2-F**)) having geometries that resemble **1** and **2**, respectively.

Table 3
Interaction energies (kcal/mol) calculated at RHF and MP2/cc-pVTZ levels of theory and polarization dispersion energy (kcal/mol)

Model	RHF	MP2	Polarisation dispersion
m1-H	6.45	−0.49	−4.96
m1-F	8.30	1.02	−6.16
m2-H	17.04	2.52	−11.79
m2-F	−8.17	−18.25	−11.61

Table 4
Partitioning of the interaction energies (kcal/mol) using the Morokuma scheme [20]

Interaction	**m1-H**	**m1-F**	**m2-H**	**m2-F**
Electrostatic	7.49	−4.88	−0.74	−25.50
Exchange	10.48	25.75	35.92	35.25
Polarisation	−11.07	−12.12	−16.47	−16.46
Charge transfer	−4.60	−6.41	−13.09	−12.36
Coupling term	1.81	3.44	8.13	7.60
Total	4.11	5.78	13.76	−11.46

the electrostatic contribution makes this geometry the most stable, compared to **m1-F**. It can be concluded that in **2** the orientation of the chloride *trans* to the PPh_3 ligand, may be ascribed to the attractive electrostatic interaction between the anion and the fluorinated phenyl rings. In **1**, which lacks this electrostatic interaction, the chloride atom is placed *trans* to C_{ipso}, due to steric hindrance.

3.2. Electronic spectra

The electronic properties of **1** and **2** are sensitive to the π-acceptor properties of the substituents directly bound to the phosphorus [6]. The UV–Vis spectra of **1** and **2** in CH_2Cl_2 solution (Fig. 6) are dominated by absorptions, not assigned uniquely before [6], which position depend only slightly on the nature of the solvent. Introduction of electron-withdrawing C_6F_5-groups in **2** results in a shift of its electronic transitions to higher energy compared to that of **1**. TD-DFT calculations have been performed to assign the experimental features of the UV–Vis spectra. To the best of our knowledge this is the first time that the TD-DFT approach has been applied to investigate the spectroscopic properties of E,C,E-pincer (E = N, P, O, S) complexes. Interestingly, the results show that the

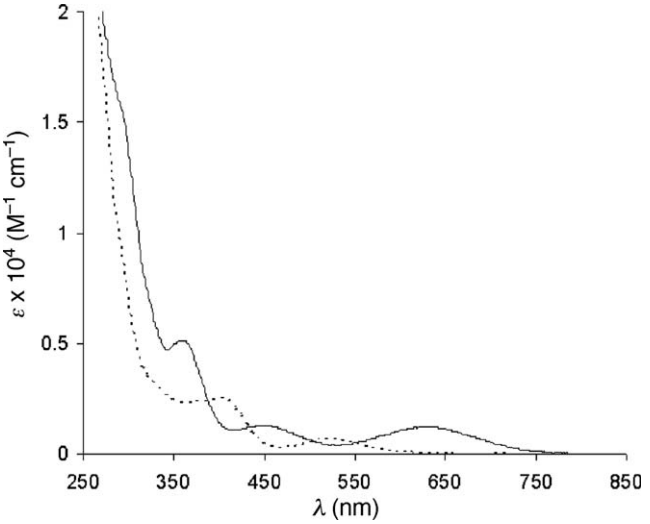

Fig. 6. UV–Vis absorption spectra of complex **1** (——) and complex **2** (- - - - -) measured in CH_2Cl_2 at 298 K [6].

TD-DFT approach is able to reproduce reasonably well the absorption bands observed experimentally in the case of **2**. All the transition energies calculated for **1** are underestimated. This might be ascribed to the use of a small basis set or to possible multireference character [11]. RPA calculations, performed using the Stuttgart RCS ECP basis set [22] for ruthenium and Dunning for other atoms [14], gave essentially identical results. Thus, this underestimation is not caused by the incorrect asymptotic behaviour of the exchange correlation functional [11]. The calculated absorptions for **1** and **2** which are associated with their excitation energies and oscillator strengths, as well as their assignments, are given in Table 5.

To clearly discuss the absorption spectra, a contour plot of the frontier orbitals involved in the assigned transitions, have been presented in Fig. 7.

A comparison between the frontier orbitals of **1** and **2** shows that the three highest occupied molecular orbitals of both complexes are very similar and have dominant contribution from the ruthenium. The HOMO of **1** and **2** is mainly localised on the metal and partly on the π orbitals of the PCP-pincer ring and on the chloride. The HOMO − 1 of both complexes resides mainly on the metal and on the chloride while their HOMO − 2 are exclusively metal in character. By contrast, the LUMO of **1** differs significantly from the LUMO of **2**: the first is exclusively localised on the metal and the second is ligand in character. The LUMO + 2 of **2** possesses mainly metal character, while the remaining low-lying unoccupied orbitals are mainly localised on the ligands.

Based on the above description of the frontier orbitals, the transitions calculated for **1** can be assigned as followed: the lowest energy band at 633 nm can be ascribed to the transitions to the 2A state having predominantly d–d character. The band at 449 nm can be attributed to the transitions to the 4A state and possesses exclusively d–d character. The transitions calculated at 383, 355, 352, 350 and 349 nm may all contribute to the experimental broad and poorly resolved band at 359 nm. However, the larger contribution comes from the transition to the 9A state, having $\pi^*_{Ru/Cl/PCP} \rightarrow \pi^*_{PCP}$ (MLCT/L′LCT) character and oscillator strength of 0.017.

Table 5
TD-DFT excitation energies (*E*) and non-vanishing oscillator strengths (*f*) calculated for **1** and **2**

State	Composition	Wavelength (nm)	Experimental λ_{max} (nm)	*f*
Compound ***1***				
2A	92% (H → L)	816	633	0.007
4A	90% (H-2 → L)	570	449	0.004
6A	32% (H-1 → L + 2)	383	359	0.023
	18% (H-1 → L + 17)			
	16% (H-1 → L + 1)			
8A	86% (H → L + 3)	355		0.003
9A	36% (H-4 → L)	352		0.017
	12% (H-5 → L)			
10A	58% (H-1 → L + 1)	350		0.008
	13% (H-1 → L + 3)			
11A	48% (H-3 → L)	349		0.005
	19% (H-6 → L)			
	11% (H → L + 5)			
Compound ***2***				
2A	30% (H → L + 5)	559	523	0.004
	17% (H → L + 7)			
	15% (H → L + 3)			
	11% (H → L + 4)			
3A	65% (H → L + 2)	528		0.003
	14% (H → L)			
6A	44% (H-1 → L + 2)	458	403	0.007
	15% (H-2 → L + 2)			
7A	34% (H-2 → L + 2)	440		0.012
	14% (H-1 → L + 2)			
10A	23% (H-1 → L + 5)	394		0.008
	14% (H-1 → L + 3)			
	11% (H-1 → L + 7)			

According to the obtained TD-DFT results (Table 5), the lowest energy band at 523 nm in the spectrum of **2** arises mainly from the $\pi^*_{Ru/Cl/PCP} \rightarrow \pi^*_{Ru/PCP}$ excitations to the 2A and 3A states and can be assigned as having predominantly d–d and partly metal-to-ligand-charge-transfer (MLCT) character. Therefore, its position is not affected to a great extent by the nature of the substituents on the phosphorus atoms and by the arrangement of the ligands around the Ru(II) centre. The band at 403 nm, formed from the excitations to the 6A, 7A and 10A states, possesses also predominant d–d character.

The DFT calculations reveal that the replacement of the C_6H_5 groups for C_6F_5 causes a decrease of the energy of the molecular $\pi^*_{Ru/PCP}$ orbitals whereas the energies of the d(Ru) orbitals remain the same. The red shift of the lowest energy transition in the spectrum of **1**, compared to what is observed in the spectrum of **2**, can be understood by taking in consideration their construction starting from the models **1cat** and **2cat**. In **1**, steric hindrance forces the chloride to be located in a position *trans* to C_{ipso}. To form **1**, the chloride has to interact with the LUMO + 1 of **1cat**,

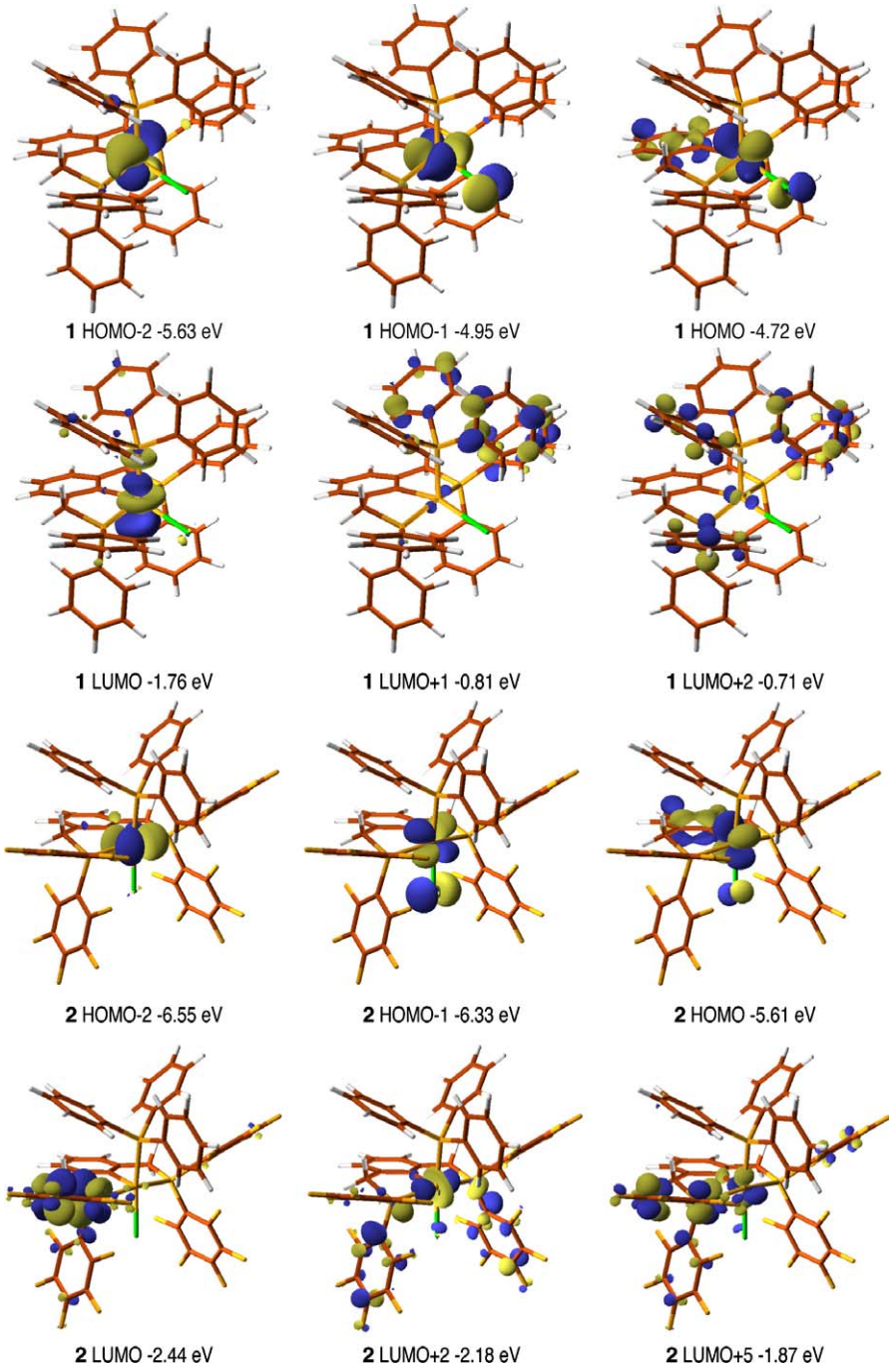

Fig. 7. Selected frontier orbitals involved in the lowest transitions of **1** and **2**.

leaving the LUMO of **1cat** the LUMO of **1**. In contrast, to form **2**, the chloride interacts with the LUMO of **2cat**. This results in a smaller gap between occupied and virtual orbitals in **1** than in **2**. An interesting consequence is that **1** is expected to be more reactive than **2**, which is indeed observed [6].

4. Conclusions

Our calculations establish that in **1** repulsive steric hindrance between the C_6H_5-rings and the chloride forces the anion to be located in position *trans* to the C_{ipso} atom. As a result, the PPh_3 ligand occupies the apical position of the square pyramidal arrangement. In **2**, attractive electrostatic interactions between the axial C_6F_5-rings and the chloride allow the anion to be located *trans* to the PPh_3 ligand and C_{ipso} in the apical position.

The UV–Vis spectroscopic features of **1** and **2** have been interpreted with the TD-DFT method. These calculations show that for both complexes the lowest energy transition has predominantly d–d character. The nature of the substituents on the phosphorus atoms, as well as the change

of the local arrangement of the ligands around the ruthenium centre, caused by steric interactions, results in a smaller energy gap between the frontier orbitals in **1**. This is reflected in the shift of its absorption bands to lower energy with respect to **2** and in its higher reactivity. Analysis of the TD-DFT calculations indicate that the exchange-correlation functional B3LYP is appropriate to get satisfactory results for the absorption spectra. However, the transition energies calculated for **1** are underestimated. Further studies should be devoted to the accurate calculation of absorption spectra of **1** and PCP-pincer Ru(II) complexes having analogous structural features.

Acknowledgements

The authors kindly acknowledge Dr. J. H. van Lenthe (Utrecht University) for helpful discussion. This work was supported by the Council for Chemical Sciences from the Netherlands Organization for Scientific Research (NWO). R.W.A.H. acknowledges financial support from NWO Grant No. 700.53.401. The authors acknowledge NWO/NCF for use of supercomputer time on TERAS, SARA, The Netherlands (Project No. SG-032).

References

[1] (a) F. Liu, E.B. Pak, B. Singh, C.M. Jensen, A.S. Goldman, J. Am. Chem. Soc. 121 (1999) 4086;
(b) M. Albrecht, G. van Koten, Angew. Chem., Int. Ed. 41 (2001) 3750;
(c) S. Gibson, D.F. Foster, G.R. Eastham, R.P. Tooze, D.J. Cole-Hamilton, Chem. Commun. (2001) 779;
(d) M.E. van der Boom, D. Milstein, Chem. Rev. 103 (2003) 1759;
(e) J.T. Singleton, Tetrahedron 59 (2003) 1837;
(f) I. Göttker-Schnetmann, P.S. White, M. Brookhart, J. Am. Chem. Soc. 126 (2004) 1804;
(g) N. Solin, J. Kjellgren, K.J. Szabó, J. Am. Chem. Soc. 126 (2004) 7026;
(h) N. Solin, O.A. Wallner, K.J. Szabó, Org. Lett. 6 (2005) 689;
(i) A. Ray, K. Zhu, Y.V. Kissin, A.E. Cherian, G.W. Coates, A.S. Goldman, Chem. Commun. (2005) 3388.

[2] (a) L.A. van de Kuil, D.M. Grove, R.A. Gossage, J.W. Zwikker, G. van Koten, Organometallics 16 (1997) 4985;
(b) R.A. Gossage, L.A. van de Kuil, G. van Koten, Acc. Chem. Res. 31 (1998) 423;
(c) D. Milstein, Pure Appl. Chem. 75 (2003) 445.

[3] P. Dani, T. Karlen, R.A. Gossage, S. Gladiali, G. van Koten, Angew. Chem., Int. Ed. 39 (2000) 743.

[4] D. Amoroso, A. Jabri, G.P.A. Yap, D.G. Gusev, E.N. Dos Santos, D.E. Fogg, Organometallics 23 (2004) 4047.

[5] E. Kossoy, M.A. Iron, B. Rybtchinski, Y. Ben-David, L.J.W. Shimon, L. Konstantinovski, J.M.L. Martin, D. Milstein, Chem. Eur. J. 11 (2005) 2319.

[6] M. Gagliardo, P.A. Chase, M. Lutz, A.L. Spek, F. Hartl, R.W.A. Havenith, G.P.M. van Klink, G. van Koten, Organometallics 24 (2005) 4553.

[7] P.A. Chase, M. Gagliardo, G.P.M. van Klink, G. van Koten, Organometallics 24 (2005) 2016.

[8] (a) G. Jia, H.M. Lee, I.D. Williams, J. Organomet. Chem. 543 (1997) 173;
(b) P. Dani, G.P.M. van Klink, G. van Koten, Eur. J. Inorg. Chem. 7 (2001) 1465;
(c) M. Lutz, P. Dani, A.L. Spek, G. van Koten, Private communication to the Cambridge Crystallographic Database, refcode JUJXOB, 1999.

[9] (a) T. Karlen, P. Dani, D.M. Grove, P. Steenwinkel, G. van Koten, Organometallics 15 (1996) 5687;
(b) M.E. van der Boom, H.-B. Kraatz, L. Hassner, Y. Ben-David, D. Milstein, Organometallics 18 (1999) 3873;
(c) D.G. Gusev, F.M. Dolgushin, M.Y. Antipin, Organometallics 19 (2000) 3429;
(d) S. Medici, M. Gagliardo, S.B. Williams, P.A. Chase, S. Gladiali, M. Lutz, A.L. Spek, G.P.M. van Klink, G. van Koten, Helv. Chim. Acta 88 (2005) 694.

[10] I. Alkorta, I. Rozas, J. Elguero, J. Am. Chem. Soc. 124 (2002) 8593.

[11] A. Dreuw, M. Head-Gordon, J. Am. Chem. Soc. 126 (2004) 4007.

[12] M. Gagliardo, H.P. Dijkstra, P. Coppo, L. De Cola, M. Lutz, A.L. Spek, G.P.M. van Klink, G. van Koten, Organometallics 23 (2004) 5833.

[13] M.F. Guest, L.J. Bush, H.J. van Dam, P. Sherwood, M.J.H. Thomas, J.H. van Lenthe, R.W.A. Havenith, J. Kendrick, J. Mol. Phys. 103 (2005) 719.

[14] (a) T.H. Dunning Jr., P.J. Hay, in: H.F. SchaeferIII (Ed.), Modern Theoretical Chemistry, vol. 3, Plenum Press, New York, 1977, p. 1;
(b) W.R. Wadt, P.J. Hay, J. Chem. Phys. 82 (1985) 284;
(c) P.J. Hay, W.R. Wadt, J. Chem. Phys. 82 (1985) 299.

[15] A.E. Reed, R.B. Weinstock, F. Weinhold, J. Chem. Phys. 83 (1985) 735.

[16] E.D. Glendening, A.E. Reed, J.E. Carpenter, F. Weinhold, NBO-3.0 Program: Natural Bond Orbital/Natural Population Analysis/Natural Localized Molecular Orbital Programs.

[17] B. Liu, A.D. McLean, J. Chem. Phys. 59 (1973) 4557.

[18] S.F. Boys, F. Bernardi, Mol. Phys. 19 (1970) 553.

[19] J.H. van Lenthe, J.G.C.M. van Duijneveldt-van de Rijdt, F.B. Duijneveldt, in: Ab Initio Methods in Quantum Chemistry, Part II, in: K. Lawley (Ed.), Advances in Chemical Physics, vol. LXIX, Wiley, Chichester, 1987, p. 521, and reference cited therein.

[20] K. Kitaura, K. Morokuma, Int. J. Quantum Chem. 10 (1976) 325.

[21] DALTON: A Molecular Electronic Structure Program, Release 2.0, 2005. Available from: <http://www.kjemi.uio.no/software/dalton/dalton.html>.

[22] M. Dolg, H. Stoll, H. Preuss, R.M. Pitzer, J. Phys. Chem. 97 (1993) 5852.